Bioactive Materials 19 (2023) 499–510

Contents lists available at ScienceDirect

Bioactive Materials

journal homepage: www.keaipublishing.com/en/journals/bioactive-materials

A non-invasive smart scaffold for bone repair and monitoring

Yazhuo Huang [a,b,1], Lingyu Zhang [a,b,1], Yongrong Ji [a,b], Hongpei Deng [a,b], Mingce Long [d], Shengfang Ge [a,b], Yanjie Su [c], Siew Yin Chan [e], Xian Jun Loh [e,*], Ai Zhuang [a,b,**], Jing Ruan [a,b,***]

[a] Department of Ophthalmology, Shanghai Ninth People's Hospital, Shanghai Jiaotong University School of Medicine, Shanghai, 200011, China
[b] Shanghai Key Laboratory of Orbital Diseases and Ocular Oncology, Shanghai, 200011, China
[c] Key Laboratory of Thin Film and Microfabrication (Ministry of Education), Department of Micro/Nano Electronics, School of Electronics, Information and Electrical Engineering, Shanghai Jiaotong University, Shanghai, 200240, China
[d] Key Laboratory of Thin Film and Microfabrication Technology (Ministry of Education), School of Environmental Science and Engineering, Shanghai Jiaotong University, Shanghai, 200240, China
[e] Institute of Materials Research and Engineering (IMRE), Agency for Science, Technology and Research (A*STAR), 2 Fusionopolis Way, Innovis, #08-03, Singapore, 138634, Singapore

ARTICLE INFO

Keywords:
Carbon nanotube
Osteogenesis
Electrochemical response
Noninvasive monitoring
Tissue engineering

ABSTRACT

Existing strategies for bone defect repair are difficult to monitor. Smart scaffold materials that can quantify the efficiency of new bone formation are important for bone regeneration and monitoring. Carbon nanotubes (CNT) have promising bioactivity and electrical conductivity. In this study, a noninvasive and intelligent monitoring scaffold was prepared for bone regeneration and monitoring by integrating carboxylated CNT into chemically cross-linked carboxymethyl chitosan hydrogel. CNT scaffold (0.5% w/v) demonstrated improved mechanical properties with good biocompatibility and electrochemical responsiveness. Cyclic voltammetry and electrochemical impedance spectroscopy of CNT scaffold responded sensitively to seed cell differentiation degree in both cellular and animal levels. Interestingly, the CNT scaffold could make up the easy deactivation shortfall of bone morphogenetic protein 2 by sustainably enhancing stem cell osteogenic differentiation and new bone tissue formation through CNT roles. This research provides new ideas for the development of noninvasive and electrochemically responsive bioactive scaffolds, marking an important step in the development of intelligent tissue engineering.

1. Introduction

Self-regeneration of bone defects caused by severe trauma, surgical resection, and congenital malformation remains challenging in the clinical setting [1,2]. Current gold standard treatments for bone defects, autologous and allogenic bone transplantations [3,4], are limited by challenges such as shortage of bone tissues donors, necrosis of donor sites, donor-derived infection, etc. [5]. In addition, allogeneic bone transplantation poses a great risk of immune rejection [6]. A variety of materials have been developed as scaffold substitutes for organ regeneration particularly for bone as well as drug delivery, including metal, inorganic, organic, and composite materials [7–22]. Nevertheless, the mismatch between the rates of new bone regeneration and scaffold degradation poses adverse effects on bone defect repair [23]. In brief, premature bone regeneration may prompt the formation of a cyst and requires a second surgery. In the case of delayed bone regeneration, the scaffold would collapse earlier before bone can be regenerated on it, as the scaffold lacks physical support later [24,25]. Moreover, seed cells

Peer review under responsibility of KeAi Communications Co., Ltd.
* Corresponding authors. Department of Ophthalmology, Shanghai Ninth People's Hospital, Shanghai Jiaotong University School of Medicine, Shanghai, 200011, China.
** Corresponding author. Department of Ophthalmology, Shanghai Ninth People's Hospital, Shanghai Jiaotong University School of Medicine, Shanghai, 200011, China.
*** Corresponding author. Department of Ophthalmology, Shanghai Ninth People's Hospital, Shanghai Jiaotong University School of Medicine, Shanghai, 200011, China.
E-mail addresses: lohxj@imre.a-star.edu.sg (X.J. Loh), aizh9h@163.com (A. Zhuang), drjruan@163.com (J. Ruan).
[1] Equal contributors.

https://doi.org/10.1016/j.bioactmat.2022.04.034
Received 24 December 2021; Received in revised form 26 April 2022; Accepted 28 April 2022

from different donors vary significantly in proliferative capacities and osteogenic potentials under the complex physiological environment [26]. Therefore, monitoring cell mineralization during bone regeneration is essential to evaluate the bone repair effect (see Scheme 1).

At present, the electrochemical responsiveness of materials has attracted extensive attention as a noninvasive detecting system in continuous monitoring of interaction between cells and interfaces [27–30]. Owing to their high surface area, hollow geometry, and satisfactory electrical properties, carbon nanotubes (CNT) have been widely utilized in the fabrication of electrochemical biosensors [31]. CNT have also been reported to induce osteogenic differentiation in human adipose-derived mesenchymal stem cells and stimulate ectopic bone formation in New Zealand white rabbits [32]. In recent years, CNT have demonstrated promising potential in cell monitoring at a two-dimensional cell culture level [33]. However, pure CNT scaffolds are hampered from being developed as scaffold substitutes as they have poor biocompatibility [34]. Carboxylated CNT is a kind of biocompatible nanomaterials, the plenty of oxygen-containing groups could contribute the CNT good solubility while the delocalized π bond between C–C make CNT as a good conductor, therefore, systematically optimizing the biocompatibility and conductivity of CNT composite scaffolds is essential to develop noninvasive electrochemically responsive scaffolds.

Apart from being an effective inducer in stem cell differentiation, CNT also possess superior mechanical characteristics [35–37], having promising potential to be used as composite scaffolds for bone regeneration. Considering the advantages of CNT, they can be utilized as bioactive and electrochemically responsive materials for repairing bone defects. Biocompatible and bioactive CNT composite scaffolds were prepared by blending CNT with polymers, inorganic materials, and polysaccharides have previously been explored. Among these materials, chitosan appears to be a promising base material for scaffold preparation due to its lack of immunogenicity, superb biocompatibility, good biodegradability, and good mechanical properties [38,39]. Carboxymethyl chitosan (CMC) is of interest as it forms tough hydrogels through chemical crosslinking and can be used as biomimetic scaffolds and sustained release systems [40–42]. In terms of improving seed cell osteogenic differentiation, bone morphogenetic protein 2 (BMP2) as an effective growth factor has been known to participate in many pathways to promote differentiation and proliferation of osteoblasts [43,44]. However, the low stability of BMP2 (i.e., easy deactivation) limits its application for long-term use in bone repair [45,46]. Considering CNT's pro-differentiation role in long-term use in bone repair, simultaneously incorporating CNT and BMP2 into scaffold could enhance seed cell osteogenic differentiation and further promote tissue mineralization maximum.

In this study, bioactive and electrochemically responsive scaffolds were prepared by integrating CNT and BMP2 into chemically crosslinked CMC hydrogels. The osteogenic ability of CNT composite scaffolds was primarily detected through voltammetry and impedance measurements, and subsequently verified by systematic biological evaluations (Schematic 1). The bioactive scaffold significantly stimulated bone formation by synergizing osteogenic effects of CNT and BMP2. These CNT composite scaffolds could also monitor osteogenic differentiation level of cells effectively by detecting electrochemical signals. This study contributes new ideas in developing electrochemically responsive bioactive scaffolds that allows noninvasive, continuous monitoring of bone regeneration process, laying the foundation for developing intelligent materials for tissue engineering.

2. Experimental section

2.1. Fabrication and characterization of CNT/CMC/BMP2 scaffolds

Carbonylated CNT were obtained from the Department of Micro/Nano Electronics, School of Electronics Information and Electrical Engineering, Shanghai JiaoTong University. CNT (8%) were dispersed in ddH_2O via sonication for 1 h. Morphology of CNT was observed by scanning electron microscope (SEM) and high-resolution transmission electron microscope (TEM). The chemical properties of CNT were examined by Fourier transform infrared (FTIR) spectroscopy and Raman spectroscopy (Senterra R200-L, Bruker, Germany).

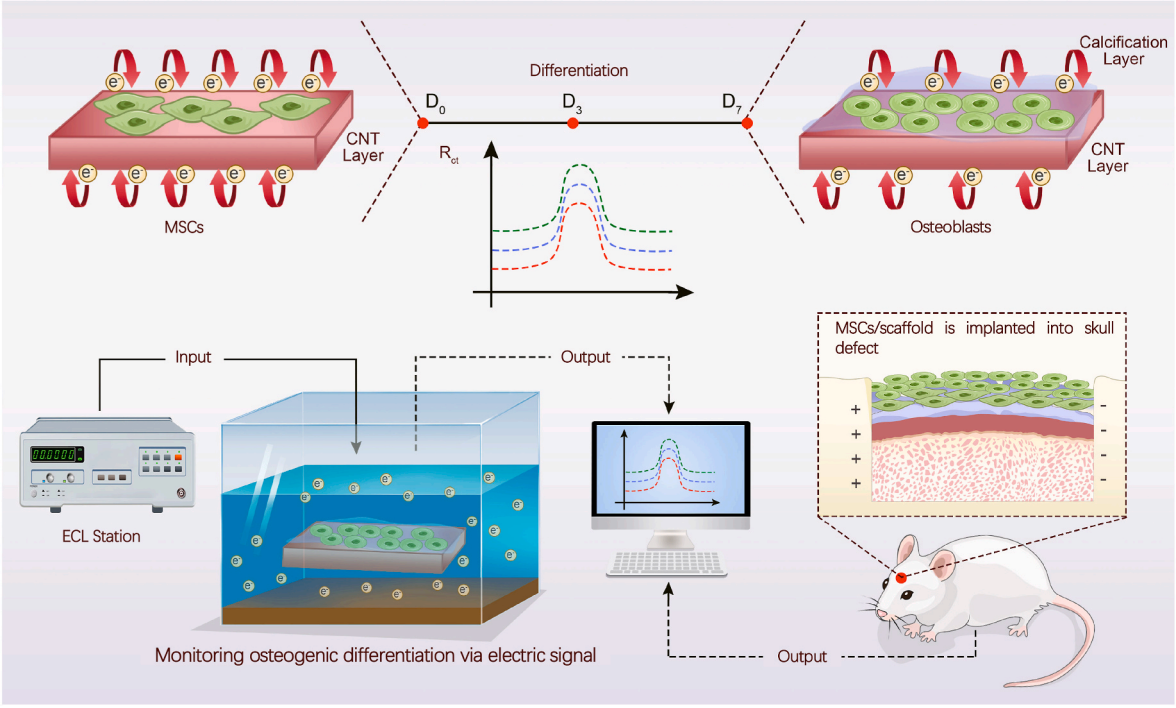

Scheme 1. Graphic of the utilization of intelligent CNT/CMC/BMP2 scaffold in noninvasive, continuous monitoring of bone regeneration (i.e., osteogenesis and mineralization).

In order to prepare CNT substrates with different concentrations, 2% CMC (2%W/V) was added to 1% and 0.5% CNT dispersion solution, respectively. The obtained solutions were mixed under magnetic stirring for 15 min and sonicated for 30 min to achieve homogeneous dispersion of CNT in CMC. Then 0.1 M N- (3-dimethylaminopropyl) -n-ethyl carbondiimide hydrochloride (EDC) and 0.025 M N hydroxyl succinimide (NHS) were added and mixed, the mixture was placed to crosslink at room temperature for 30 min and rinse twice with ddH_2O under ultrasonic washing to obtain CNT substrates. In order to prepare three-dimensional porous scaffold materials, the above obtained homogeneous CNT/CMC mixture was frozen overnight at −80 °C and lyophilized overnight, next the redundant crosslinking reagents were rinsed three times with ddH_2O under ultrasonic washing, finally the CNT composite scaffolds were obtained by re-lyophilized overnight. The CMC scaffold was prepared by self-crosslinking CMC under the action of NHS and EDC, the lyophilization and rinse procedures were referred to above operation. For BMP2-integrated CNT substrates and scaffolds, 0.25 ng/μL BMP2 was added into each CNT dispersion solution. The scaffold morphology was observed with SEM (JEOL JSM 5600LV). Chemical properties of scaffolds were characterized by performing Nicolet 6700 FTIR spectrometer (Thermo Electron Corporation, USA) and Raman spectroscopy (Senterra R200-L, Bruker, Germany). To test the mechanical performance of CNT/CMC scaffolds, 10-mm-diameter scaffolds were prepared for compression load test using a tabletop uniaxial testing instrument. Load capacity of 50 N force at a rate of 0.5 mm/min was set for the compression load test. Compressive strength and Young's modulus were calculated on the basis of the stress–strain curve of each sample.

2.2. Degradation and BMP2 release of scaffolds

For the scaffold degradation test, combing the ASTM standards (F-1635–95) and Biological Evaluation of Medical Devises- Part 13 standards (ISO 10993–13: 2010 IDT), the scaffolds were performed accelerating enzyme degradation test, briefly, the scaffolds were soaked in degradation medium of ddH_2O containing 500 μg/mL lysozyme at 65 °C, after the 1, 3, 5, 7, 10 and 14 days degradation treatment, the scaffolds were respectively rinsed with ddH_2O and lyophilized, the weight of scaffolds were measured before and after degradation treatment. For the BMP2 release rate test, the CNT/CMC/BMP2 scaffold was soaked in PBS for 1, 2, 3, 5, 7, 10 and 14 days. The supernatant was collected and measured by ELISA (R&D Systems, USA) to quantified the content of BMP2.

2.3. Isolation and subculture of human adipose-derived stem cells (hADSCs)

Based on our previous work [47], protocol involved in isolation of hADSCs was authorized by Shanghai JiaoTong University of Medicine through the Ethics Committee of Shanghai Ninth People's Hospital. Fat pads of patients aged 18–40 years old whom had received double eyelid surgeries were obtained from the department of ophthalmology. After rinsing with phosphate buffer saline (PBS) for 3 times, fat pads were cut into pieces of 1 mm^3. The fat pads were then immersed in 1 mg/mL collagenase I (Sigma Aldrich, St. Louis, MO, USA) and incubated at a 37 °C shaker overnight. Digested tissue was obtained via centrifugation at 1200 rpm for 15 min. The precipitate was resuspended in α-MEM (Invitrogen, Carlsbad, CA, USA) containing 10% fetal bovine serum (FBS) (Gibco, USA) and 1% penicillin-streptomycin (Invitrogen). The tissue mixture was then incubated at a 37 °C incubator with CO_2 atmosphere maintained at 5%. Every three days, the culture medium was replaced. They only employed cells from the third to fifth passages of growth in future studies.

2.4. Biocompatibility of CNT scaffolds

hADSCs were adjusted to a concentration of 1×10^4/100 μL and plated on substrates with different CNT contents. Cell counting kit-8 (CCK-8) assay (Dojindo, Japan) was used to enumerate the proliferation of cells cultured on substrates for 4, 24, and 72 h. Viability of hADSCs cultured on different substrates was detected using a Live/Dead kit (Invitrogen) following the manufacturer's instructions. To further validate the scaffold's biocompatibility, flow cytometry analysis was performed through the Annexin V and propidium iodide staining at third day after hADSCs coculture with scaffold. Scanning electron microscopy (SEM) examination was also performed to evaluate the biocompatibility of hADSCs seeded on the scaffold, after the cells were cultured in scaffold for 3 and 7 days, the scaffold was fixed with 2.5% glutaraldehyde for 30 min, dehydrated with a graded ethanol series, and observed using SEM.

2.5. Osteogenic differentiation and mineralization potentials of CNT scaffolds

hADSC were seeded on the scaffolds 7 days with 60–70% confluence, the total cellular RNA of hADSCs was extracted with Trizol (Sigma Aldrich, USA) reagent and reverse transcribed into cDNA with primescript RT Kit (Takara, Tokyo, Japan). The relative mRNA expression levels of bone formation-related genes, including alkaline phosphatase (ALP), bone sialoprotein (BSP), collagen alpha 1 chain type I (COL1A1), osteocalcin (OCN), and Runt-related transcription factor 2 (Runx2), were analyzed using real-time qPCR with SYBR premix ex Taq (Takara) on the 7900HT FAST real-time PCR system (Applied Biosystems, Carlsbad, California, USA). All tests were repeated at least 3 times and results were normalized based on the expression of GAPDH. Primers used in the experiments are listed in Table 1. Expression levels of osteogenesis proteins were evaluated at 14 days after culture. For the protein extraction, hADSCs were lysed on ice for 30 min in cell lysis buffer and centrifuged at 10,000 g for 15 min to collect the supernatants, the protein amount was established using bicinchoninic acid (BCA) protein assay kit (Thermo Fisher Scientific Inc., MA). The loading quantities of proteins for each sample was corrected accordingly. Proteins were first separated by 10% SDS-PAGE and transferred onto polyvinylidene difluoride (PVDF) membranes (Millipore, USA). The membranes were blocked with 5% nonfat milk for 1 h and incubated with primary antibodies (i.e., Col1A1, Runx2, OPN, BSP, OSX, OCN, and β-actin) at 4 °C overnight. The membranes were subsequently incubated with secondary antibodies (i.e., anti-rabbit or anti-mouse peroxidase-labeled antibodies (Jackson ImmunResearch, West Grove, PA, USA)) at 25 °C for an hour. After washing 3 times in TBST, the membranes were wetted with ECL plus reagent (Millipore, USA) and visualized with Tanon 5200 Multi System (Shanghai). All primary and secondary antibodies were purchased from Abcam.

After 7 days of osteogenic induction, quantitative alkaline phosphatase (ALP) was determined according to the manufacturer's instructions. Substrates and p-nitrophenol from ALP test kit (Beyotime, China) were added to cell lysates and incubated at 37 °C for 15 min. ALP activity was measured at 405 nm. ALP test and alizarin red staining were carried out after 14 and 21 days of osteogenic induction. Photos were taken after cell fixation and staining. CNT/CMCs were precoated on glass slides and hADSCs were left to differentiate for 14 days. Immunocytochemistry (ICC) was then performed. After fixation, hADSCs were blocked with PBS containing 10% goat serum for 1 h, incubated with primary antibodies (e.g., BSP and Runx2) at 4 °C overnight, and incubated with secondary antibodies at room temperature for 1 h. The nuclei were stained with Hoechst (Invitrogen) and observed with Olympus BX51 microscope.

2.6. Electrochemical assay for ALP monitoring on CNT substrates

Electrochemical assay was carried under the following three-electrode system: a platinum foil as the counter electrode, an Ag/AgCl electrode as the reference electrode, and indium tin oxide conductive

Table 1
Primer sequences.

Gene	Accession No.	Forward Primer (5′-3′)	Reverse Primer (3′-5′)
ALP	NM_001632.5	GGACATGCAGTACGAGCTGA	CCTTCCACCAGCAAGAAGAA
COL1A1	NM_000088.4	AAGAGGCGAGAGAGGTTTCC	ACCAGCATCACCCTTAGCAC
BSP	NM_004967.4	CGGAGGAGACAATGGAGAAG	CCACCATTTGGAGAGGTTGT
OCN	NM_199173.6	GGCGCTACCTGTATCAATGG	TCAGCCAACTCGTCACAGTC
OSX	NM_001173467.3	AACAACTCTGGGCAAAGCAG	CAGGTGAAAGGAGCCCATTA
Runx2	NM_001015051.4	GTGGACGAGGCAAGAGTTTC	TTCCCGAGGTCCATCTACTG
GAPDH	NM_001256799.3	CTGACTTCAACAGCGACACC	TGCTGTAGCCAAATTCGTTG

glass (ITO) with CNT/CMC scaffold as the working electrode. Cyclic voltammetry (CV) test was run under N_2 atmosphere at a scanning speed of 50 mV/s for the range of −0.2 to 0.4 V. The surfaces of ITO were first scraped. ITO were then coated with cross-linked CNT/CMC mixture within 2 min and dried overnight in a 60 °C oven. hADSCs were seeded on dried CNT/CMC substrates and left for incubation for 2, 5, and 10 days. hADSCs/CNT/CMC were incubated in 0.2 mM pAPP at 37 °C for 45 min prior to CV test. The standard curve of ALP response to peak current values was obtained by testing 0.2 mM P-aminophenyl phosphate (pAPP) (Aladdin, Shanghai) solutions containing different concentration of ALP (Sigma-Aldrich, USA) incubated at 37 °C for 45 min with three-electrode system.

2.7. Electrochemical response of CNT scaffolds to cells differentiation

Electrochemical detection system of cells differentiation was set up as follows: a counter electrode using a platinum wire was used. SCE (saturated calomel electrode) was used as a reference electrode. Electrolyte consists of 3 mM potassium ferricyanide (0.1 g $K_3Fe(CN)_6$/100 mL) and 0.1 M potassium chloride (0.745 g KCl/100 mL) was prepared. CV test was run under N_2 atmosphere at a scanning speed 50 mV/s for the range of −0.1 to 0.6 V. Electrochemical impedance spectroscopy (EIS) test was run under N_2 atmosphere with applied bias of +0.2 V and AC amplitude of 5 mV for frequency range of 0.1–10^5 Hz. Two-dimensional and three-dimensional electrode systems were constructed as mentioned above. hADSCs were seeded and incubated on two- and three-dimensional electrode systems. After trypsin digestion, the electrodes were stored in ddH_2O and detected by the above electrochemical system.

2.8. Electrochemical response of CNT scaffolds to cranial defect repair

Protocols were authorized by the Shanghai Jiaotong Medical University's Ninth People's Hospital's animal research committee. A cranial defect model of eight-week male SD rats was used to test the electrochemical response of CNT/CMC scaffolds *in vivo*. Before surgery, scaffolds were seeded with hADSCs and grown for three days. Two critical size defects were created on both sides of SD rat skulls with a 5-mm-diameter trephine (Nouvage company, Golddaher, Switzerland). The defects were subsequently filled up using scaffolds and cell composites. Based on the number of weeks since transplantation, 12 rats were randomly assigned to one of four groups: CNT/CMC-1 week, CNT/CMC-2 week, CNT/CMC-3 week, and CMC-3 week. The SD rats were sacrificed after the predefined period and scaffolds were retrieved from the skulls and tested for CV and EIS performance after trypsin digestion.

2.9. Bone defect repair study of scaffolds

Protocols were authorized by the Shanghai Jiaotong Medical University's Ninth People's Hospital's animal research committee. hADSCs/scaffold were implanted into SD rat skull defects to examine the osteogenic capacity of CNT scaffolds. CNT/CMC/BMP2 rats were arbitrarily separated into four groups, as were CNT/CMC rats, CMC group as well as the NC group. Intraperitoneal administration of tetracycline (1 mg/kg body weight) was given at week 2, Alizarin Red S (3% in 2% sodium bicarbonate solution, 0.8 mL/kg body weight) at week 4, and Calcine (1% in 2% sodium bicarbonate solution, 5 mL/kg body weight) at week 6 (all from Sigma) An animal micro-CT scanner (mCT-80, Scanco Medical, Switzerland) was utlized to analyze the structure of rebuilt skulls in high-resolution scanning mode. The 3D isosurface reconstruction tool was then used to examine the skulls. Results from a micro-CT scan were examined using the percentage of new bone volume (BV/TV), the number of trabeculae (Tb. N), and bone mineral density (BMD).

Animals were killed 8 weeks following surgery in order to study the bone growth of scaffolds. The skulls were collected, fixed with 4% PFA, and dehydrated in 75–100% ethanol solutions. To perform histological staining, the samples were implanted into polymethylmethacrylate (PMMA). As a rule, the thickness of each slice is 40 nm. We utilized a Leica TCS SP8 microscope with the Leica Las AF software to view cells at 488 nm, 543 nm, and 405 nm (calcium yellow green, red, and blue) (tetracycline, yellow). Van Gieson's picrofuchsin was then applied to the samples. A light microscope was used to examine the new bone's volume and location.

2.10. Statistical analysis

Each experiment was repeated for at least 3 times. All data were shown as mean ± SD unless otherwise specified. Data were analyzed by one-way ANOVA. $P < 0.05$ was statistically significant.

3. Results and discussion

3.1. Characterization of the CNT composite scaffolds

TEM revealed that CNT could dispersed in water and have a diameter ranged from 6 to 10 nm (Fig. 1a and b). Raman spectroscopy was performed to verify the electronic structure of carbon atoms in CNT (Fig. 1c). D band at 1340 cm^{-1} and G band at 1572 cm^{-1} represent the specific characteristics of CNT. R value (I_D/I_R) illustrates the number of chemical groups on the surface of CNT. After chemical crosslinking with CMC, the R value of CNT decreased as the chemical groups on the surface had become occupied. The chemical groups of CNT were characterized by FTIR (Fig. 1d). Absorption peaks at ~3400 and 1370 cm^{-1} were induced by O–H stretching and bending vibrations, respectively. Absorption peaks of C–H stretching modes in CNT can be observed at 2920 cm^{-1}. The peaks at 1730, 1621, and 1064 cm^{-1} represent stretching modes of C═O and C═C, respectively. The bending mode of C–O illustrates that CNT are carboxylated and could be beneficial for the preparation of CNT/CMC scaffolds.

CNT/CMC scaffolds were prepared by chemically crosslinking CNT and CMC through amide reaction. SEM images showed that both pristine CMC and CNT/CMC scaffolds possess interconnected porous structures and the latter with a pore size ranged from 50 to 80 μm (Fig. 2a), which would allow better cell communication and nutrient transportation [48]. Incorporation of CNT (0.5% w/v) could improve the mechanical properties of CMC scaffold (Fig. 2c). Compared to pristine CMC scaffold, the compressive strength and Young's modulus of CNT-doped scaffold increased by 7.25-fold from 0.4408 ± 0.07951 kPa to 3.2 ± 0.4438 kPa and 7.19-fold from 1.075 ± 0.1931 kPa to 7.733 ± 0.9905 kPa, respectively (Fig. 2d and e). What is more, the degradation curve of

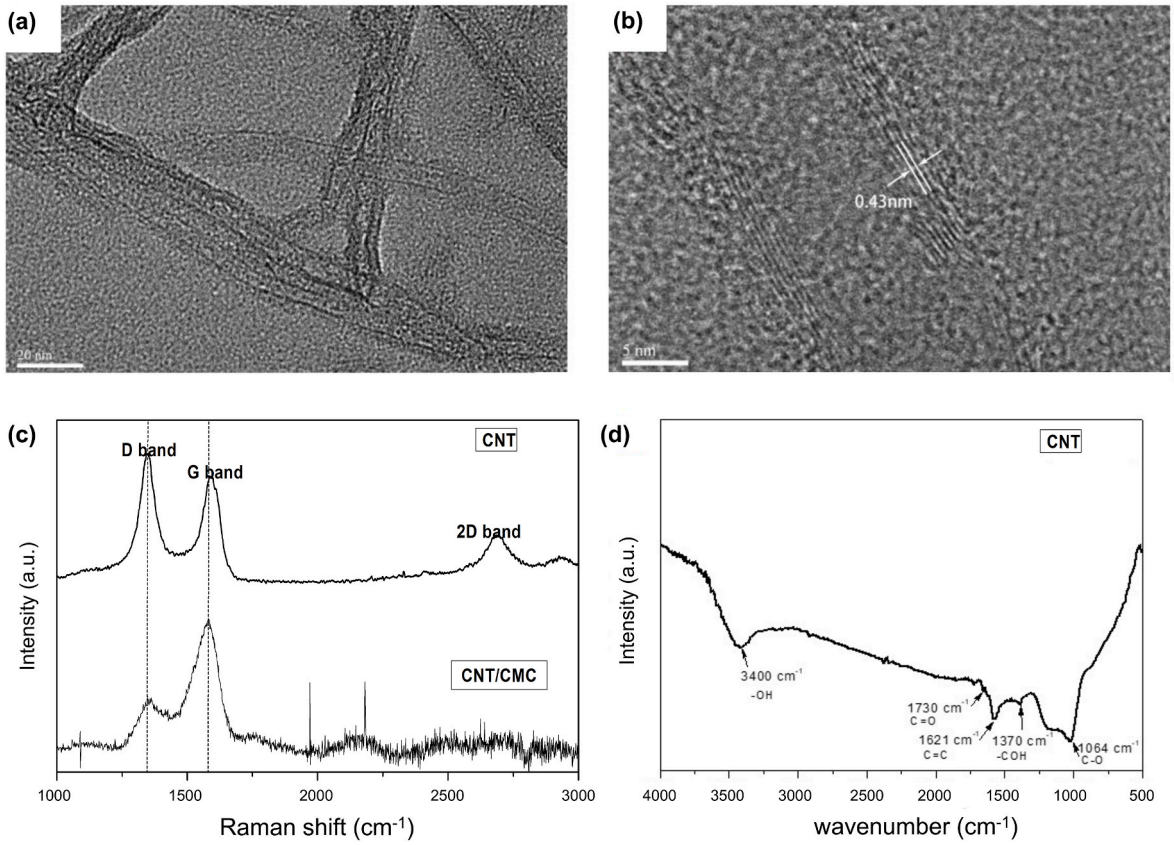

Fig. 1. Characterization of CNT. a) and b) TEM and high resolutions images of CNT; c) Raman spectrum of CNT; d) FTIR spectrum of CNT.

scaffold illustrated that CNT/CMC is a sustained degradable biomaterial (Fig. 2b).

3.2. Optimization of biocompatible CNT scaffolds and its osteogenic differentiation potential

Incorporation of CNT may improve the bioactivity and electrochemical sensitivity of scaffolds, but it also poses a risk of toxicity. Therefore, optimizing the concentration of CNT in the system is important to prepare biocompatible, bioactive, and electrochemical response-sensitive scaffolds. Final CNT concentration was chosen based on the biocompatibility and osteoinductivity tests of scaffolds. A CCK-8 assay was used to detect the proliferation rate of hADSCs planted on different substrates, including 0%, 1%, and 0.5% (w/v) CNT composite substrates. Results showed that there was little proliferation in the first 24 h in both 1% and 0.5% groups, presumably due to acute stress reaction. As the culturing time was prolonged to 72 h, the proliferation rate of CNT groups increased with 0.5% group higher than 1% group. Both CNT groups proliferated slower than the group with CMC (Fig. 3a), that is because the CNT has good promoting cells differentiation effect. In order to learn more about the safety of CNT/CMC scaffolds, hADSCs were stained with Live/Dead assay after they were cultured with 0.5% CNT/CMC scaffolds for 3 days. Results showed that CNT/CMC scaffolds and substrates are biocompatible as there were almost no dead cells after cultured with them (Figs. 3b and S1a). The cells in the CNT/CMC groups were clustered together while cells in the CMC group were relatively dispersed because the cells were more inclined to differentiate under CNT stimulation. The flow cytometry analysis results showed that 96.95% of the cells are survival after 3 days culture (Fig. S1b). SEM revealed that the cells were in wide spindle shapes (Fig. 3c), showing that CNT/CMC scaffolds have good adhesive capability to the cells and allows them to grow well [49].

ALP is an important marker of early osteogenesis [50]. To evaluate the osteogenic differentiation potential of CNT/CMC scaffolds, ALP assay was applied a week after cells were grown on CMC and CNT/CMC scaffolds. Results showed that 0.5% CNT/CMC scaffold had significant pro-osteogenic ability while there was no significant difference between 1% CNT/CMC and CMC scaffolds (Fig. 3d). mRNA expression levels of osteogenic-related genes, i.e. *ALP*, *BSP*, *COL1A1*, *OCN* and *OSX*, showed similar trends (Fig. 3e–i). Taken account of the good biocompatibility and osteoinductivity of 0.5% CNT/CMC scaffold, 0.5% CNT was selected as the optimal concentration for subsequent experiments.

3.3. Osteogenic differentiation potential of the CNT scaffold in vitro

In the early phase of osteogenesis, osteogenic differentiation of cells is limited due to restricted contact between seed cells and CNT. Addition of BMP2 into the system could synergistically stimulate the osteogenic differentiation of seed cells. As BMP2 could be rapidly deactivated, it could be designed to sustained release in a short term to initiate differentiation of seed cell. The BMP2 release curve indicated that BMP2 could sustainably release from CNT/CMC/BMP2 scaffold in 14 days (Fig. S5). By degrading the CNT/CMC scaffold, exposed CNT could maintain the osteogenic differentiation direction of cells for a long term [51]. mRNA expression levels of osteogenic-related genes were increased in CNT/CMC/BMP2 scaffold compared with CNT/CMC scaffold (Fig. 4a–d). Bone formation-related proteins expression levels were analyzed using Western blot after hADSCs incubated on different samples for 14 days. Results showed that osteogenesis-related proteins (i.e., Col1A1, Runx2, OPN, BSP, OSX, and OCN) were expressed higher in CNT/CMC/BMP2 group than CNT/CMC group, while CMC group had the lowest proteins expression levels (Fig. 4e and f).

To better evaluate the ontogenetic potential of CNT/CMC/BMP2, ALP and ARS staining were performed after hADSCs grown on different

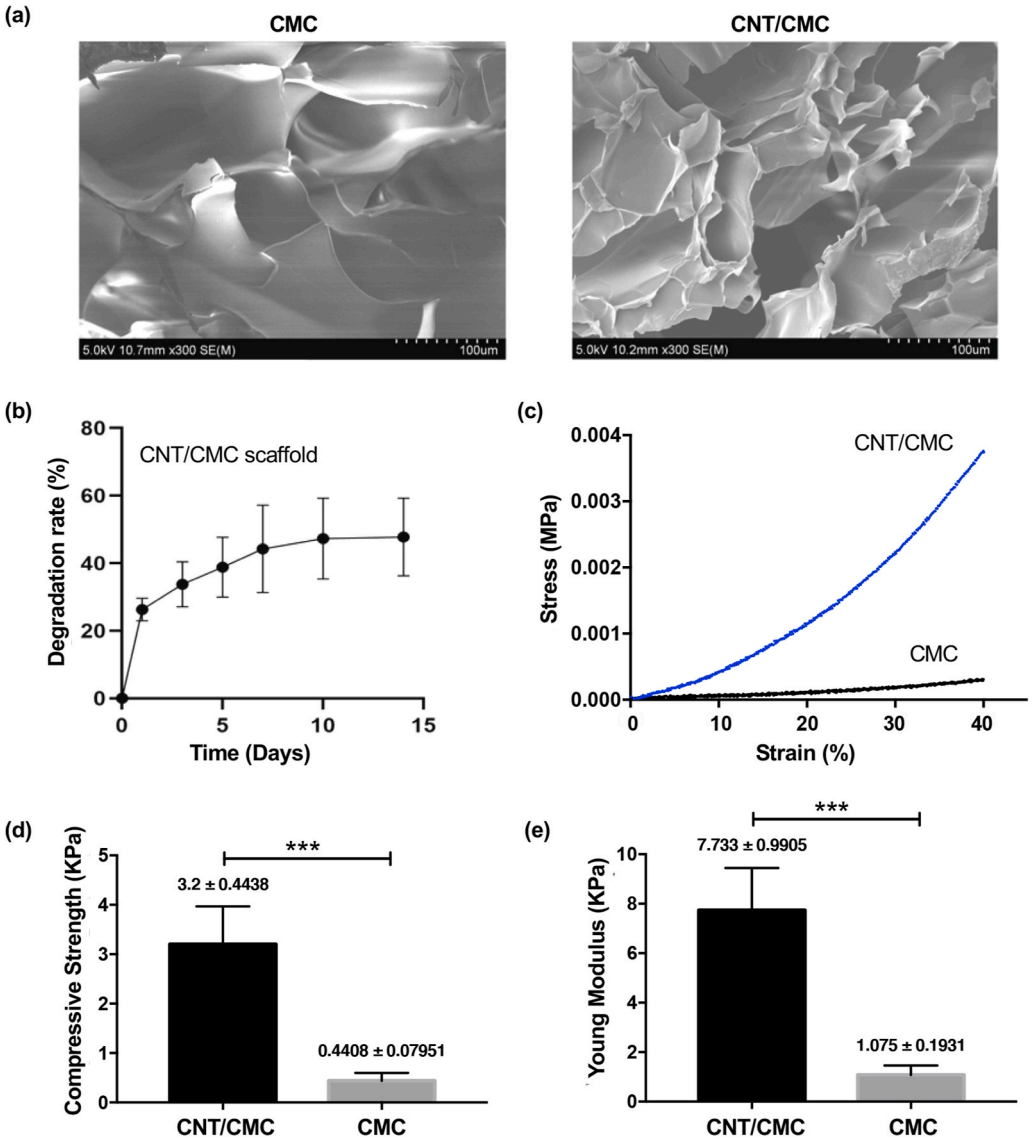

Fig. 2. Microstructure and mechanical properties of the scaffolds. a) SEM Images of the pristine CMC and CNT/CMC scaffold; b) Degradation curve of the scaffold; c) stress–strain curve of the scaffold; d) Young's modulus and e) compressive strength of the scaffold (***P < 0.001).

samples for 2 and 3 weeks. ALP and ARS examination revealed that CNT/CMC/BMP2 group exhibited enhanced ALP activity and significant mineralization ability, respectively (Fig. 4g and h). Immunocytochemistry staining of hADSCs was further conducted after 14 days of incubation. Results showed that expression levels of osteogenic transcription factor Runx2 and cytoplasmic protein BSP were higher in CNT/CMC/BMP2 group compared to both CNT/CMC and CMC groups (Fig. S2). These results demonstrated that CNT/CMC/BMP2 group showed enhanced osteogenic differentiation potential as compared to CNT/CMC group.

3.4. Electrochemical response of CNT scaffolds during cell osteogenic differentiation

Electrochemical sensitivity of CNT composite scaffolds is critical in monitoring osteogenic differentiation of cells. CV and EIS were used to evaluate the degree of cell osteogenic differentiation after seeding hADSCs onto CNT electrodes. The osteogenic potential of CNT/CMC scaffold was first proven by electrochemical sensing of ALP generation. ALP, an important osteogenesis marker, was able to catalyze electrochemical inactive P-aminophenyl phosphate (pAPP) to produce active p-aminophenol (pAP), and the redox pair of pAP/quinone imine could generate oxidation/reduction peak on CV curves (Fig. 5a). The CV diagram reflects the electrode reversible redox reaction degree. A higher peak current derivation value implies a better redox characteristic [52]. CV curve of pure pAPP presented no peak. With ALP addition, distinct oxidation/reduction peaks with similar altitudes appeared, suggesting a reversable redox process. To obtain the correlation between ALP concentrations and peak current values, different amount of ALP was added into pAPP and tested for CV performance on CNT/CMC scaffold (Fig. S3). The linear regression showed that concentration of ALP and oxidation peak current value (Ip_{ox}) have a positive correlation with a R^2 of 0.98. The value of CV basal current also increased with higher concentration of ALP (Fig. 5b), presumably due to the enhanced electron transfer efficiency on electrode surface by the ALP generated redox pairs. For determining the potential of osteogenesis differentiation induction of the CNT/CMC scaffold, equal amount of hADSCs were seeded on CNT/CMC substrates and incubated for 0, 2, 5, and 10 days. These hADSCs/CNT/CMC substrates were pretreated with pAPP before CV tests. Compared with 0-day group, oxidation peak started to appear in 2-, 5-, 10-day groups and the value of Ip_{ox} and basal current was gradually improved with prolonged incubation time (Fig. 5c and d). The

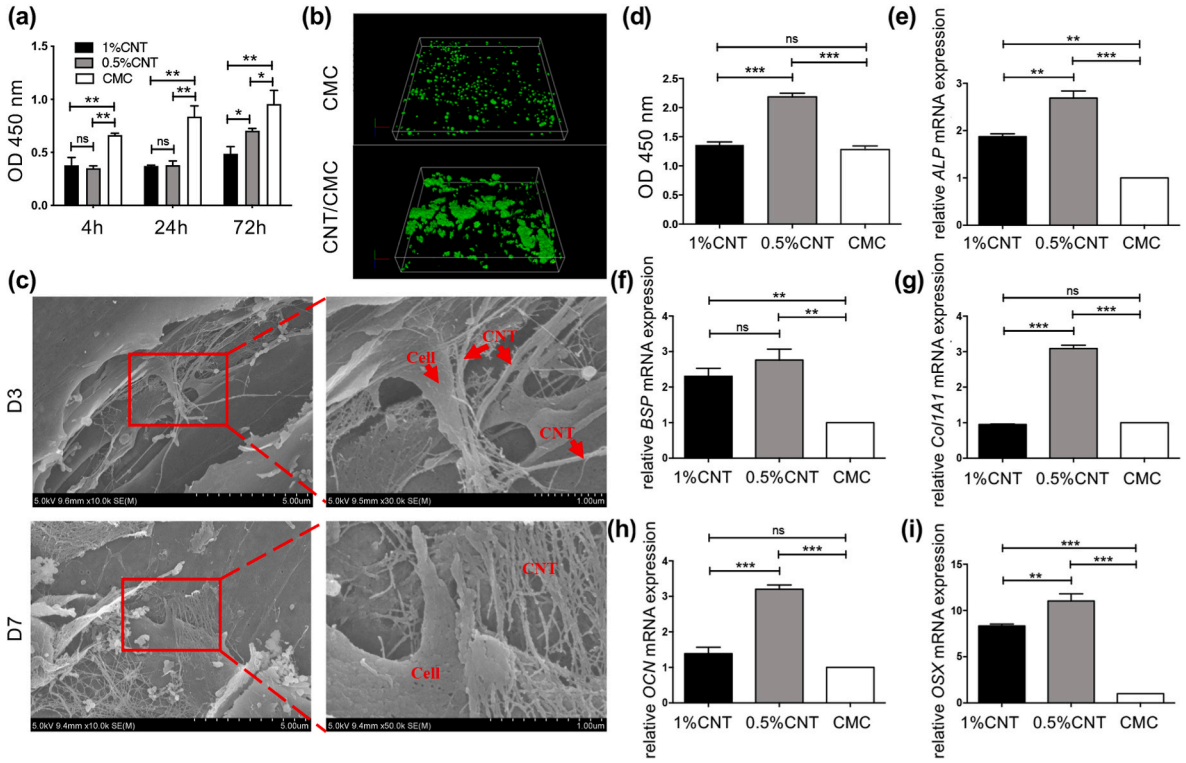

Fig. 3. Osteoinductive effects of varying quantities of CNT in a CNT/CMC matrix. a) Propagation of hADSCs on CNT/CMC and CMC samples for 72 h; b) Live/Dead assay profile of hADSCs cultured on 0.5% CNT/CMC and CMC samples for 3 days (merged signals); c) hADSCs incubated on 0.5% CNT/CMC scaffolds for 3 and 7 days; d) ALP quantitative analysis of hADSCs in 1% CNT/CMC, 0.5% CNT/CMC and CMC scaffolds; e-i) expression levels of osteogenesis-specific genes (*ALP, BSP, Col1A1, OCN and OSX*) of hADSCs cultured on samples for a week. GAPDH has been used to standardize the data from three separate investigations. (*P < 0.05, **P < 0.01, ***P < 0.001).

longer hADSCs incubated on CNT/CMC scaffold, the more ALP could be produced in extracellular matrix on the electrode surface. As ALP are secreted during early osteogenesis, results demonstrated that CNT/CMC scaffold facilitated hADSCs osteogenesis differentiation and the differentiation process tended to be more mature with longer incubation time. It also illustrated that CNT/CMC could be used as a potential electrode with good inductivity and sensitivity on detecting seed cells osteogenesis.

To further evaluate CNT-induced osteogenic differentiation capability and electrochemical signals sensing ability, EIS curves were plotted after 0-, 3- and 7-day differentiation culture of hADSCs on CNT/CMC substrate. The smaller the diameter of the arc, the lower the charge transfer resistance (R_{ct}) [53,54]. EIS curve showed that the R_{ct} of 7-day differentiated group was considerably greater than that of 3- and 0-day differentiated group (Fig. 5e). As most of the extracellular matrix but not the mineralization matrix could be removed through trypsin digestion, changes in electrochemical signals could be seen as the mineralization matrix deposition degree. When the charge transfer ability of hADSCs/CNT/CMC decreased with prolonged cell differentiation time, it means CNT could enhance hADSC osteogenic differentiation and induce cells to form a mineralizing matrix. The CV curve showed the redox characteristic of hADSCs/CNT/CMC in descending order from the control group to the 7-day group (Fig. 5f), indicating that the 7-day group electrodes have low peak current value due to the influence of the cell mineralization matrix. Evaluation on the conductivity and osteogenic capability of the three-dimensional CNT scaffolds were also carried out. CV and EIS measurements of CNT/CMC scaffold were recorded after seeding hADSCs for 1 and 2 weeks. As the cell culturing time increased, the conductivity of CNT/CMC scaffold decreased significantly, as reflected in EIS curve that the R_{ct} increasing from the control group to the 2-weeks group (Fig. 5g). Meanwhile, the CV results also showed that CNT/CMC scaffold had a lower peak current value after culturing cells for 2 weeks compared with the 1-week and control groups (Fig. 5h). Both CV and EIS results suggest that CNT/CMC scaffolds are feasible as an osteogenic induction and/or monitoring platform with electrochemical-responsive signal. In addition, to further validate BMP2 acts early osteogenesis promotion effects on cells in an electrochemical manner, the CV peak current tended to decrease and R_{ct} exhibited increased as the hADCSs incubation time prolonged in CNT/CMC/BMP2 scaffold (Fig. 5i and j). More importantly, comparison of the CV and EIS results of CNT/CMC and CNT/CMC/BMP2 scaffolds, CNT/CMC/BMP2 group presented a lower CV peak current and higher Rct at the first and second week after seeded hADSCs (Fig. S4), the results illustrated that the CNT/CMC/BMP2 scaffold processed a better ability on promoting early osteogenesis and larger effect on forming mineralizing matrix compared with CNT/CMC scaffold. Meanwhile, CV and EIS curves of the scaffolds were almost coincided whatever supplement with and without BMP2 before seeding hADSCs (Fig. S4), it implied that addition of BMP2 would not interfere electrochemical response of the scaffolds.

3.5. *Electrochemical monitoring of early osteogenic differentiation on CNT scaffold in cranial defect rats*

Since CNT/CMC scaffold revealed the potential of electrochemical monitoring cellular osteogenic differentiation, the effectiveness of the scaffold's electrochemical response was further validated after transplantation *in vivo* (Fig. 6a), CV and EIS curves of CNT/CMC scaffold were harvested and recorded on week 0, 1, 2, and 3 after transplantation into cranial defects of rat (Fig. 6b). The peak value of current in CV curve declined gradually and the diameter of EIS increased gradually for prolonged duration of placement *in vivo*. These reflect reduction in the scaffold's electroconductivity, presumably due to mineralization matrix deposition (Fig. 6c and d). In contrast, CMC scaffold exhibited almost no changes in electrochemical signal response with limited potential in

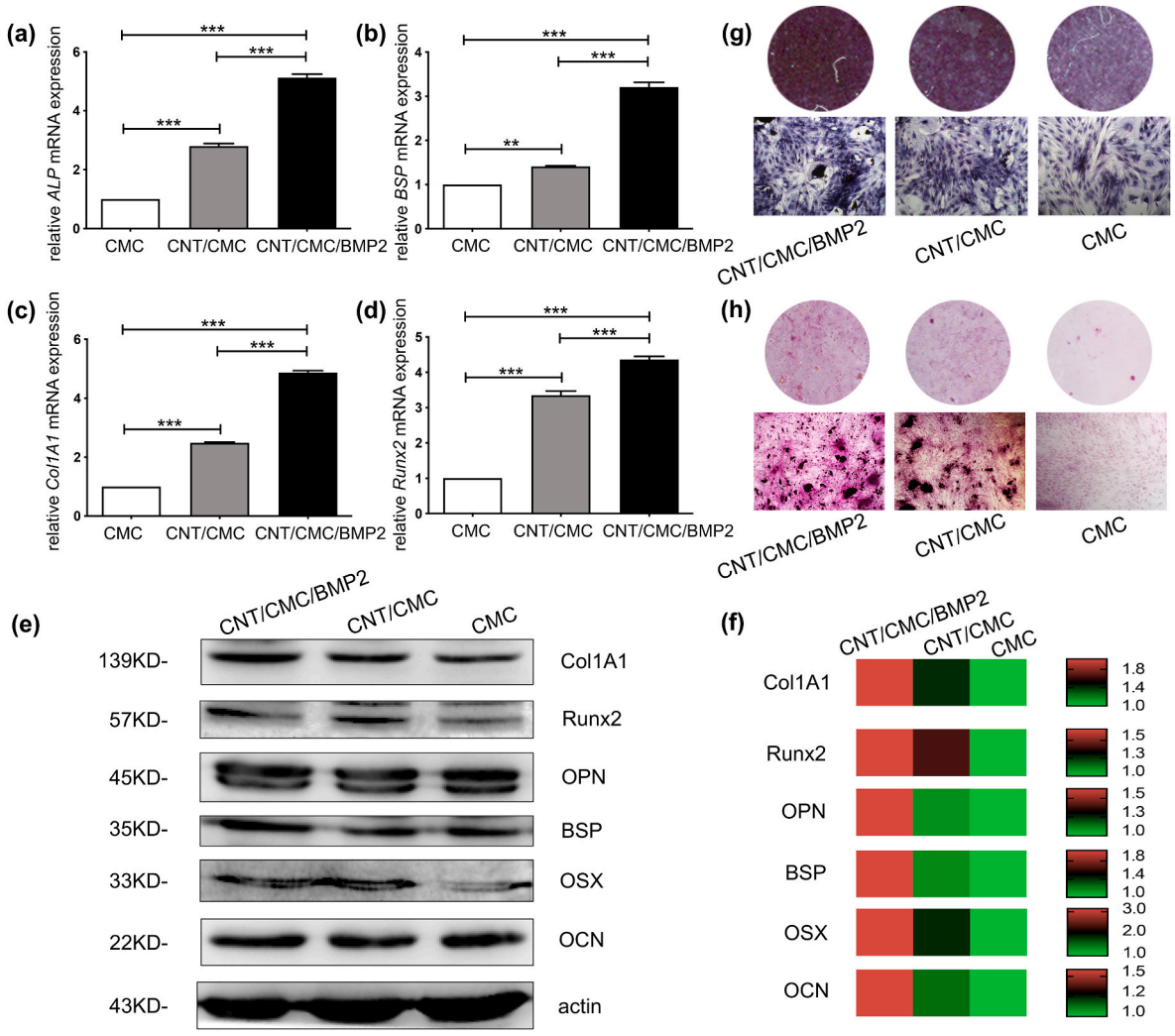

Fig. 4. Assessment of the osteogenic differentiation of hADSC CNT/CMC/BMP2 samples. a-d) Levels of osteogenesis-specific genes (ALP, BSP, Col-1 and Runx2) as expressed in hADSCs cultured on substrates a week; e) Proteins expression levels and f) quantitative analysis of osteogenic markers(Col1A1, Runx2, OPN, BSP, OSX and OCN)after hADSCs cultured on substrates 2 weeks; g) ALP and h) ARS staining of hADSCs cultured on substrates for 2 and 3 weeks. The data shown represent the mean of three separate trials and standardized to GAPDH (*P < 0.05, **P < 0.01, ***P < 0.001).

osteogenic induction (Fig. 6e). Compared with CNT/CMC scaffold, the changes of CMC scaffold's CV and EIS curve were insignificant after 3 weeks' transplantation. At the same time, it also proved that electrochemical signal variation of CNT/CMC scaffold was mainly derived from the early osteogenic differentiation (Fig. 6f and g). These results indicated that CNT/CMC scaffold retained good sensitivity for electrochemical monitoring of early osteogenic differentiation *in vivo*.

3.6. Bone defect repairing effects of CNT scaffolds in vivo

The osteoinductivity of CNT/CMC scaffold was evaluated using a critical-size calvarial defect model. hADSCs were seeded onto the scaffolds 3 days before the surgery and transplanted into 5-mm-diameter bone defects in SD rats' skulls. The high-resolution micro-CT imaging revealed the presence of bone abnormalities during an 8-week transplant period. Bone tissues developed in CNT/CMC/BMP2 group had almost covered all bone defects. There was a reduced amount of bone tissues produced in both CNT/CMC and CMC groups and virtually no new bone tissues developed in the NC group (Fig. 7a). These had been validated with quantitative morphometric examination of osteogenesis as well as the new bone volume to tissue volume ratio (BV/TV). The CNT/CMC/BMP2 group had a greater BV/TV ratio of 33.28 ± 6.03% as compared to CNT/CMC (12.31 ± 3.20%), CMC (6.144 ± 1.73%), and NC (3.859 ± 3.54%) groups (Fig. 7b). The trabecular number (Tb. N) of CNT/CMC/BMP2 group (2.227 ± 0.77 per mm) was significantly greater than CNT/CMC (1.157 ± 0.80 per mm), CMC (0.2097 ± 0.14 per mm), and NC (0.3015 ± 0.07 per mm) groups (Fig. 7c). Bone mineral density (BMD) analysis additionally confirms that a greater amount of new bone tissues was developed in CNT/CMC/BMP2 group (0.34 ± 0.13 g/cc) than in CNT/CMC (0.17 ± 0.08 g/cc), CMC (0.03 ± 0.04 g/cc), and NC (0.03 ± 0.03 g/cc) groups (Fig. 7d). It appears that CNT/CMC/BMP2 scaffold had superior osteoinductivity than either CNT/CMC and CMC scaffolds.

To study the mineralization ability of scaffolds at the histological level, the fluorescent dyes tetracycline, alizarin red S, and calcein were injected into SD rats to mark the different stages of new bone formation at 2, 4, and 6 weeks after surgery, respectively. Representative images of each group showed that bone repair effect of CNT/CMC/BMP2 group was better than those of CNT/CMC, CMC, and NC groups at all stages of osteogenesis (Fig. 7e). Fluorescence intensity quantitative analysis results revealed that CNT/CMC/BMP2 group (1.39 ± 0.56%) had a higher percentage of tetracycline (yellow) than CNT/CMC (1.07 ± 0.45%), CMC (0.36 ± 0.22%), and NC (0.21 ± 0.25%) groups (Fig. 7f). The percentage of alizarin red S (red) in the CNT/CMC/BMP2 group was 2.9 ± 0.79%, while the percentages in CNT/CMC, CMC and NC groups were 1.82 ± 0.68%, 0.6 ± 0.29%, and 0.58 ± 0.27%, respectively (Fig. 7g).

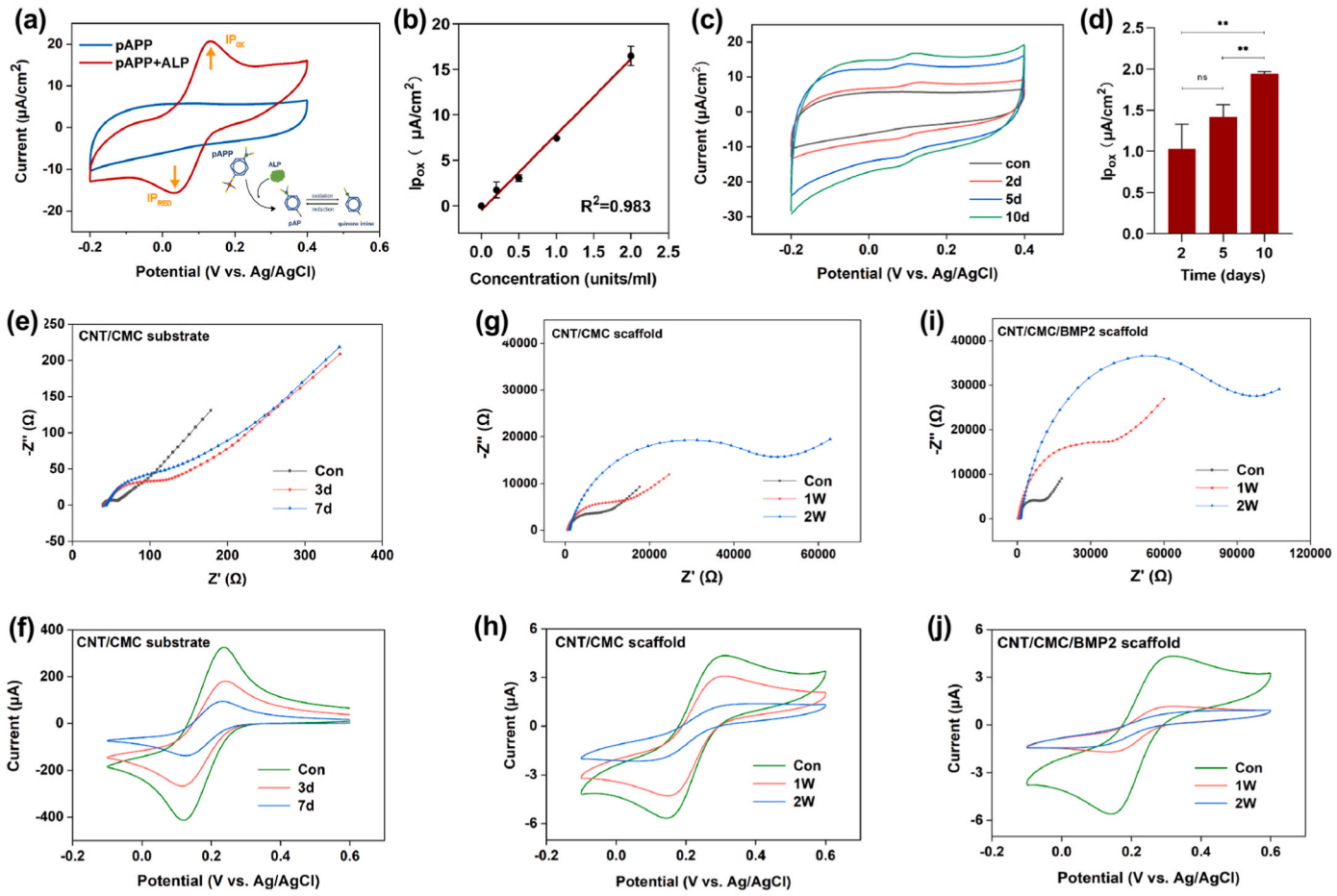

Fig. 5. Electrochemical signal response to CNT/CMC substrate and scaffold during osteogenic differentiation *in vitro*. a) Schematic of redox pair generation by ALP and the CV response of pAPP with and without ALP; b) Linear regression of ALP concentrations and oxidation peak currents (Ip_{ox}); c) CV response and d) Ip_{ox} of hADSCs/CNT/CMC substrate after 0, 2, 5 and 10 days culture; e) EIS and f) CV curve of the hADSCs/CNT/CMC substrate after 0, 3 and 7 days of culture; g) EIS and h) CV of the hADSCs/CNT/CMC scaffold after 1 and 2 weeks culture; i) EIS and j) CV curve of the hADSCs/CNT/CMC/BMP2 scaffold after 1 and 2 weeks culture.

There was also substantial variation in the percentage of calcein (green) between the CNT/CMC/BMP2 (2.95 ± 0.22%), CNT/CMC (1.63 ± 0.41%), CMC (0.75 ± 0.30%), and NC (0.37 ± 0.24%) groups (Fig. 7h). From these results, it showed that CNT/CMC/BMP2 scaffold had the best bone-promoting effect out of all the scaffolds tested.

Arrangement of collagen fibers is one of the main process that occurs during new bone formation. Collagen fibers occupy the most organic part of the bone and combine with the inorganic component to realize mineralization [55–57]. Therefore, the content of collagen fibers can directly reflect tissue mineralization effect. Herein, collagen fibers were stained by van Gieson's picrofuchsin to evaluate the mineralization degree in new tissues. The representative sagittal view images indicated that the gap was almost filled by collagen fibers in CNT/CMC/BMP2 group, which was better than the results in the CNT/CMC group, while there was almost no collagen signal in CMC and NC groups (Fig. 7i). Collectively, *in vivo* experiment of bone defect repair demonstrated that CNT/CMC/BMP2 had promising potential as bone defect repair scaffolds with enhanced osteoinductivity.

4. Conclusion

Monitoring early mineralization of tissue is beneficial in evaluating the effectiveness of scaffolds. A novel bioactive CNT composite scaffold was fabricated by integrating CNT into chemically crosslinked CMC hydrogels. The CNT composite scaffold exhibited sensitive electrochemical response signals to seed cell osteogenic differentiation and tissue mineralization in both cellular and animal levels. Incorporation of BMP2 could synergistically induce new bone formation with CNT. CNT could counterbalance the shortcoming of BMP2 for long-term bone tissue formation. Development of bioactive and electrochemically responsive CNT composite scaffolds lays the foundation for long-term noninvasive, continuous monitoring of newly formed tissues in regenerative medicine.

Funding

This work was supported by the National Natural Science Foundation of China (81972530, 62171275, 82000879), the National Key R&D Project (2018YFC1106100 and 2018YFC1106101), Fund for Excellent Young Scholars of Shanghai Ninth People's Hospital, Shanghai Jiao Tong University School of Medicine (JYYQ001), and the Science and Technology Commission of Shanghai (20DZ2270800).

Conflicts of interest

No potential conflicts of interest were reported by the authors.

Availability of data and material

The raw data and materials were available upon request.

Code availability (software application or custom code)

Not applicable.

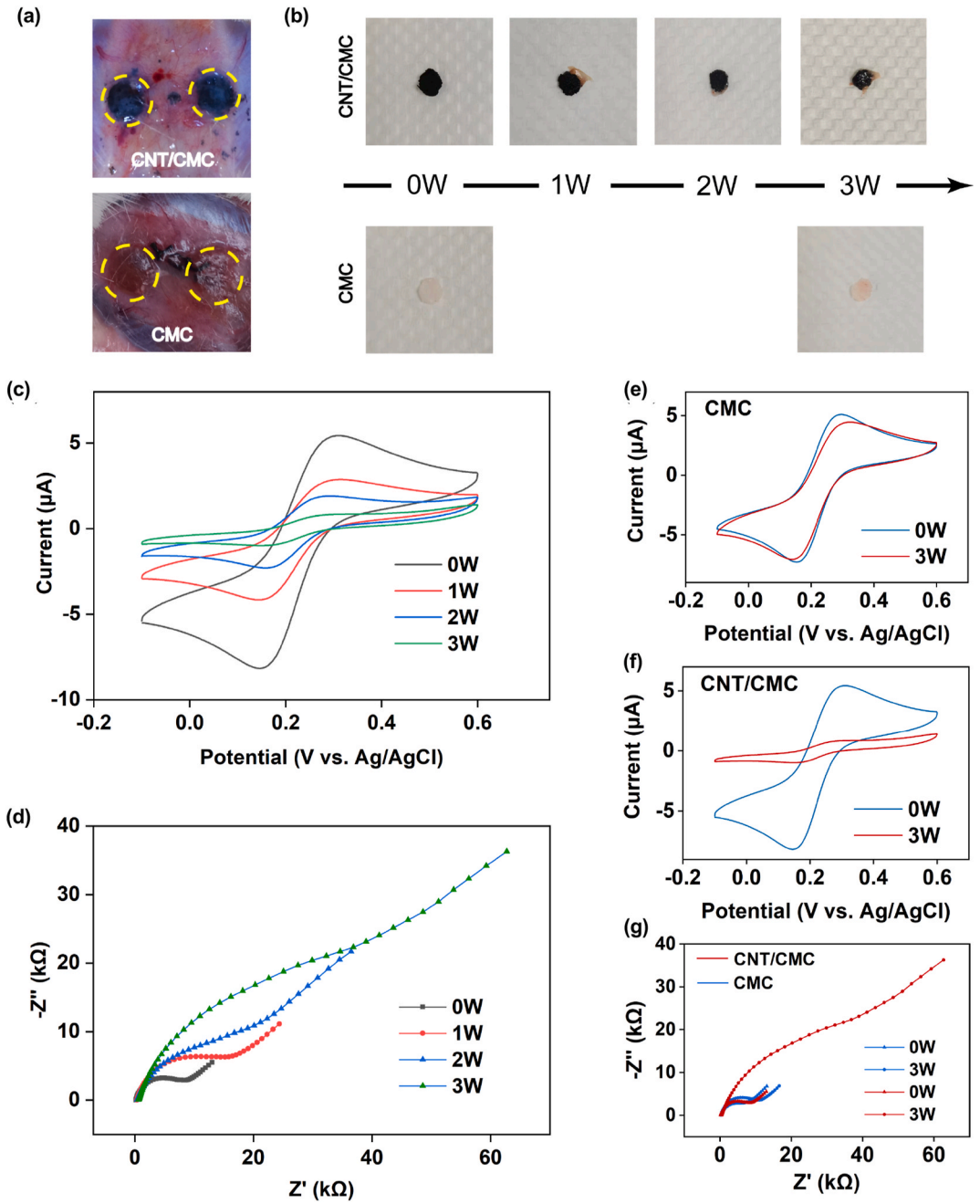

Fig. 6. Electrochemical signal response to CNT/CMC scaffold during osteogenic differentiation *in vivo*. a) *In vivo* images of CNT/CMC scaffold (upper) and CMC scaffold (down) after 3-weeks' transplantation in rat's skull; b) The retrieved CNT/CMC and CMC scaffold after 0-, 1-, 2- and 3-weeks' transplantation; c) CV response and d) EIS curve of CNT/CMC scaffold after 0-, 1-, 2- and 3-weeks' transplantation to bone defect of rat's skull; Comparing CV response of e) CMC scaffold and f) CNT/CMC scaffold after 0- and 3-weeks' transplantation to rat's skull; g) Comparing EIS response of CMC and CNT/CMC scaffold after 0- and 3-weeks' transplantation to rat's skull.

Authors' contributions

JR designed the research and approved the manuscript; YZH performed the experiments with assistance from LYZ, YRJ, HPD, YJS and MCL; AZ and JR supervised the experiments; YZH, XJL, SYC drafted the manuscript; JR, XJL, SYC edited the manuscript; LYZ, XJL, SYC and SFG analyzed the data. All the authors read and approved this manuscript.

Ethics approval

This research was performed in accordance with the World Medical Association Declaration of Helsinki. Written informed consent was obtained from all patients. The study and procedures for care and use of animals were approved by the Ethics Committee of Shanghai Ninth People's Hospital, Shanghai JiaoTong University School of Medicine and all applicable institutional and governmental regulations concerning the ethical use of animals were followed.

CRediT authorship contribution statement

Yazhuo Huang: performed the experiments with assistance from LYZ. **Lingyu Zhang:** SYC, and . **Yongrong Ji:** and. **Hongpei Deng:** and. **Mingce Long:** and, JR supervised the experiments; YZH, XJL. **Shengfang Ge:** analyzed the data. All the authors read and approved this

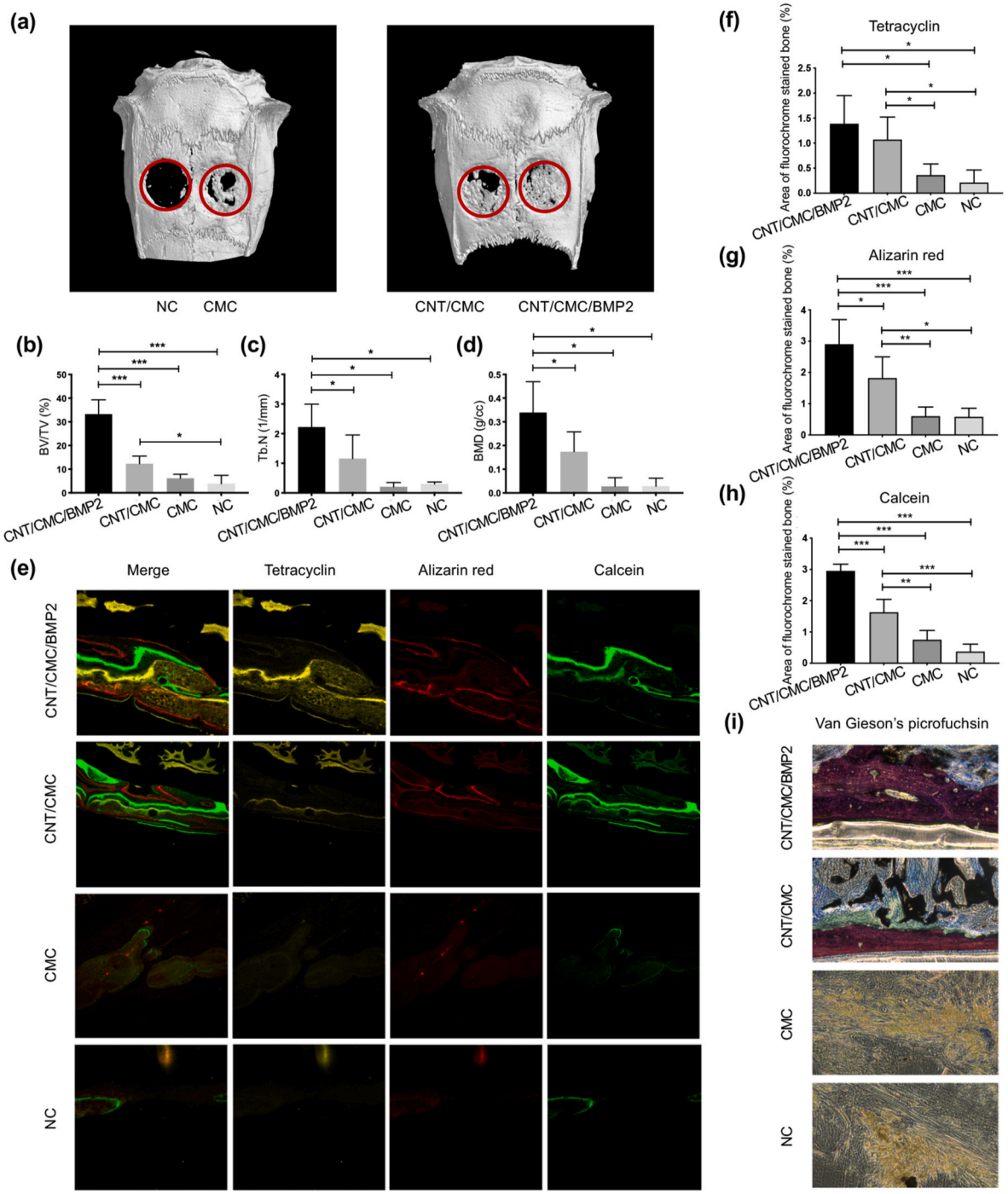

Fig. 7. Assessment of the potential of bone repair of CNT/CMC/BMP2 scaffold. a) Micro-CT imaging examination of critical-sized rat calvarial defects 8 weeks post-implantation; b) BV/TV, c) Tb.N and d) BMD examination of the freshly formed bone; e) fluorochrome-labeled images and f-h) quantitative examination of new bone formation and mineralization; i) histological assessment of the sliced specimens; the newly formed bone was stained red with van Gieson's picrofuchsin (*P < 0.05, **P < 0.01, ***P < 0.001).

manuscript. **Yanjie Su:** and. **Siew Yin Chan:** drafted the manuscript, JR, XJL, SYC, edited the manuscript. **Xian Jun Loh:** SYC, and . **Ai Zhuang:** and, JR supervised the experiments; YZH, XJL. **Jing Ruan:** designed the research and approved the manuscript.

Appendix A. Supplementary data

Supplementary data to this article can be found online at https://doi.org/10.1016/j.bioactmat.2022.04.034.

Protocols were authorized by the Shanghai Jiaotong Medical University's Ninth People's Hospital's animal research committee. hADSCs/scaffold were implanted into SD rat skull defects to examine the osteogenic capacity of CNT scaffolds. CNT/CMC/BMP2 rats were arbitrarily separated into four groups, as were CNT/CMC rats, CMC group as well as the NC group. Intraperitoneal administration of tetracycline (1 mg/kg body weight) was given at week 2, Alizarin Red S (3% in 2% sodium bicarbonate solution, 0.8 mL/kg body weight) at week 4, and Calcine (1% in 2% sodium bicarbonate solution, 5 mL/kg body weight) at week 6 (all from Sigma) An animal micro-CT scanner (mCT-80, Scanco Medical, Switzerland) was utlized to analyze the structure of

rebuilt skulls in high-resolution scanning mode. The 3D isosurface reconstruction tool was then used to examine the skulls. Results from a micro-CT scan were examined using the percentage of new bone volume (BV/TV), the number of trabeculae (Tb. N), and bone mineral density (BMD).

Animals were killed 8 weeks following surgery in order to study the bone growth of scaffolds. The skulls were collected, fixed with 4% PFA, and dehydrated in 75–100% ethanol solutions. To perform histological staining, the samples were implanted into polymethylmethacrylate (PMMA). As a rule, the thickness of each slice is 40 nm. We utilized a Leica TCS SP8 microscope with the Leica Las AF software to view cells at 488 nm, 543 nm, and 405 nm (calcium yellow green, red, and blue) (tetracycline, yellow). Van Gieson's picrofuchsin was then applied to the samples. A light microscope was used to examine the new bone's volume and location.

References

[1] A.A. El-Rashidy, J.A. Roether, L. Harhaus, U. Kneser, A.R. Boccaccini, Acta Biomater. 62 (2017) 1–28.
[2] S. Patel, J.-M. Caldwell, S.B. Doty, W.N. Levine, S. Rodeo, L.J. Soslowsky, S. Thomopoulos, H.H. Lu, J. Orthop. Res. 36 (2018) 1069–1077.
[3] H.C. Pape, A. Evans, P. Kobbe, J. Orthop. Trauma 24 (2010).
[4] L. Karalashvili, A. Kakabadze, M. Uhryn, H. Vyshnevska, K. Ediberidze, Z. Kakabadze, Georgian Med. News (2018) 44–49.
[5] M.L. Azi, A. Aprato, I. Santi, M. Kfuri Jr., A. Masse, A. Joeris, BMC Muscoskel. Disord. 17 (2016) 465, 465.
[6] G.A. Ahmed, B. Ishaque, M. Rickert, C. Fölsch, Orthopä 47 (2018) 52–66.
[7] K. Rezwan, Q.Z. Chen, J.J. Blaker, A.R. Boccaccini, Biomaterials 27 (2006) 3413–3431.
[8] Y. Zhang, J.R. Venugopal, A. El-Turki, S. Ramakrishna, B. Su, C.T. Lim, Biomaterials 29 (2008) 4314–4322.
[9] C. Deng, R. Lin, M. Zhang, C. Qin, Q. Yao, L. Wang, J. Chang, C. Wu, Adv. Funct. Mater. 29 (2019) 1806068.
[10] Z. Zheng, Y. Chen, H. Hong, Y. Shen, Y. Wang, J. Sun, X. Wang, Advanced Healthcare Materials 10 (2021) 2000631.
[11] P. Cai, B. Hu, W.R. Leow, X. Wang, X.J. Loh, Y.L. Wu, X. Chen, Adv. Mater. 30 (2018) 1800572.
[12] X. Fan, J.Y. Chung, Y.X. Lim, Z. Li, X.J. Loh, ACS Appl. Mater. Interfaces 8 (2016) 33351–33370.
[13] X. Liu, X. Chen, M.X. Chua, Z. Li, X.J. Loh, Y.L. Wu, Advanced Healthcare Materials 6 (2017) 1700159.
[14] X.J. Loh, J. Appl. Polym. Sci. 127 (2013) 992–1000.
[15] X.J. Loh, W. Guerin, S.M. Guillaume, J. Mater. Chem. 22 (2012) 21249–21256.
[16] X.J. Loh, V.P.N. Nguyen, N. Kuo, J. Li, J. Mater. Chem. 21 (2011) 2246–2254.
[17] X.J. Loh, Z.-X. Zhang, K.Y. Mya, Y.-l. Wu, C.B. He, J. Li. *Journal of Materials Chemistry* 20 (2010) 10634–10642.
[18] X. Su, M.J. Tan, Z. Li, M. Wong, L. Rajamani, G. Lingam, X.J. Loh, Biomacromolecules 16 (2015) 3093–3102.
[19] J. Wang, L. Tian, B. Luo, S. Ramakrishna, D. Kai, X.J. Loh, I.H. Yang, G.R. Deen, X. Mo, Colloids Surf. B Biointerfaces 169 (2018) 356–365.
[20] Y.L. Wu, H. Wang, Y.K. Qiu, S.S. Liow, Z. Li, X.J. Loh, Advanced healthcare materials 5 (2016) 2679–2685.
[21] Y. Xiang, N.N.L. Oo, J.P. Lee, Z. Li, X.J. Loh, Drug Discov. Today 22 (2017) 1318–1335.
[22] D.P. Yang, M.N.N.L. Oo, G.R. Deen, Z. Li, X.J. Loh, Macromol. Rapid Commun. 38 (2017) 1700410.
[23] J.E. Dumas, E.M. Prieto, K.J. Zienkiewicz, T. Guda, J.C. Wenke, J. Bible, G.E. Holt, S.A. Guelcher, Tissue Eng. 20 (2014) 115–129.
[24] S. Saravanan, R.S. Leena, N. Selvamurugan, Int. J. Biol. Macromol. 93 (2016) 1354–1365.
[25] L. Roseti, V. Parisi, M. Petretta, C. Cavallo, G. Desando, I. Bartolotti, B. Grigolo, Mater Sci Eng C Mater Biol Appl 78 (2017) 1246–1262.
[26] R.C. Nordberg, J. Zhang, E.H. Griffith, M.W. Frank, B. Starly, E.G. Loboa, Stem Cells Transl Med 6 (2017) 502–511.
[27] C. Sengiz, G. Congur, E. Eksin, A. Erdem. *Electroanalysis* 27 (2015) 1855–1863.
[28] Y. Yang, H. Zhang, C. Huang, D. Yang, N. Jia, Biosens. Bioelectron. 89 (2017) 461–467.
[29] A. Zhang, W. Guo, H. Ke, X. Zhang, H. Zhang, C. Huang, D. Yang, N. Jia, D. Cui, Biosens. Bioelectron. 101 (2018) 219–226.
[30] Y. Luo, W. Li, Q. Lin, F. Zhang, K. He, D. Yang, X.J. Loh, X. Chen, Adv. Mater. 33 (2021) 2007848.
[31] M.M. Barsan, M.E. Ghica, C.M.A. Brett, Anal. Chim. Acta 881 (2015) 1–23.
[32] Z. Du, X. Feng, G. Cao, Z. She, R. Tan, K.E. Aifantis, R. Zhang, X. Li, Bioact. Mater. 6 (2021) 333–345.
[33] I. Suzuki, M. Fukuda, K. Shirakawa, H. Jiko, M. Gotoh, Biosens. Bioelectron. 49 (2013) 270–275.
[34] A. Eatemadi, H. Daraee, H. Karimkhanloo, M. Kouhi, N. Zarghami, A. Akbarzadeh, M. Abasi, Y. Hanifehpour, S.W. Joo, Nanoscale Res. Lett. 9 (2014) 393.
[35] P. Newman, A. Minett, R. Ellis-Behnke, H. Zreiqat, Nanomedicine 9 (2013) 1139–1158.
[36] B. Pei, W. Wang, N. Dunne, X. Li, Nanomaterials 9 (2019) 1501.
[37] M. Tanaka, K. Aoki, H. Haniu, T. Kamanaka, T. Takizawa, A. Sobajima, K. Yoshida, M. Okamoto, H. Kato, N. Saito, Nanomaterials 10 (2020) 659.
[38] S.D. Kozusko, C. Riccio, M. Goulart, J. Bumgardner, X.L. Jing, P. Konofaos, J. Craniofac. Surg. 29 (2018) 1788–1793.
[39] A. Oryan, S. Sahvieh, Int. J. Biol. Macromol. 104 (2017) 1003–1011.
[40] R. Jayakumar, M. Prabaharan, R.L. Reis, J.F. Mano, Carbohydr. Polym. 62 (2005) 142–158.
[41] S. Sharmeen, A.F.M.M. Rahman, M.M. Lubna, K.S. Salem, R. Islam, M.A. Khan, Bioact. Mater. 3 (2018) 236–244.
[42] W. Hu, Z. Wang, Y. Xiao, S. Zhang, J. Wang, Biomater Sci 7 (2019) 843–855.
[43] S.S. Lee, B.J. Huang, S.R. Kaltz, S. Sur, C.J. Newcomb, S.R. Stock, R.N. Shah, S. I. Stupp, Biomaterials 34 (2013) 452–459.
[44] W. Zhang, G. Yang, X. Wang, L. Jiang, F. Jiang, G. Li, Z. Zhang, X. Jiang, Adv. Mater. 29 (2017) 1703795.
[45] B. Tabisz, W. Schmitz, M. Schmitz, T. Luehmann, E. Heusler, J.C. Rybak, L. Meinel, J.E. Fiebig, T.D. Mueller, J. Nickel. *Biomacromolecules* 18 (2017) 695–708.
[46] H. Lin, Y. Tang, T.P. Lozito, N. Oyster, B. Wang, R.S. Tuan, Stem Cell Res. Ther. 10 (2019) 254.
[47] Y.-z. Huang, Y.-r. Ji, Z.-w. Kang, F. Li, S.-f. Ge, D.-P. Yang, J. Ruan, X.-q. Fan, Chem. Eng. J. 395 (2020) 125098.
[48] T. Toyoda, S. Mae, H. Tanaka, Y. Kondo, M. Funato, Y. Hosokawa, T. Sudo, Y. Kawaguchi, K. Osafune, Stem Cell Res. 14 (2015) 185–197.
[49] Z. Yu, C. Xiao, Y. Huang, M. Chen, W. Wei, X. Yang, H. Zhou, X. Bi, L. Lu, J. Ruan, X. Fan, RSC Adv. 8 (2018) 17860–17877.
[50] K. Ino, T. Onodera, Y. Kanno, A. Suda, R. Kunikata, T. Matsue, H. Shiku, Electrochim. Acta 268 (2018) 554–561.
[51] J.H. Lee, H.K. Choi, L. Yang, S.D. Chueng, J.W. Choi, K.B. Lee, Adv Mater 30 (2018), e1802762.
[52] E.P. Randviir, C.E. Banks, Anal. Methods 5 (2013) 1098–1115.
[53] N. Elgrishi, K.J. Rountree, B.D. McCarthy, E.S. Rountree, T.T. Eisenhart, J. L. Dempsey, J. Chem. Educ. 95 (2018) 197–206.
[54] K. Sahithi, M. Swetha, K. Ramasamy, N. Srinivasan, N. Selvamurugan, Int. J. Biol. Macromol. 46 (2010) 281–283.
[55] S.H. Liu, R.S. Yang, R. al-Shaikh, J.M. Lane, Clin. Orthop. Relat. Res. (1995) 265–278.
[56] D. Zhang, X. Wu, J. Chen, K. Lin, Bioact. Mater. 3 (2018) 129–138.
[57] M. Ansari, Prog Biomater 8 (2019) 223–237.